# Crystal structure of nanocrystalline Pr5Co19 compound and its hydrogen storage properties

W. Bouzidi, L. Patout, A. Charaï, N. Mliki, Lotfi Bessais

# Crystal structure of nanocrystalline $Pr_5Co_{19}$ compound and its hydrogen storage properties

W. Bouzidi,[1,2] L. Patout,[3] A. Charai,[3] N. Mliki,[2] and L. Bessais[1]

[1)] *Université Paris Est Créteil, CNRS, ICMPE, UMR7182, F-94320, Thiais, France*

[2)] *Université de Tunis El Manar, Faculté des Sciences de Tunis, Laboratoire Matériaux Organisation et Propriétés (LR99ES17), 2092 Tunis, Tunisie*

[3)] *Aix Marseille Univ, Lab IM2NP, UMR 7334, CNRS, Fac Sci, Campus St Jerome, F-13397 Marseille, France*

The present study focuses on the structure and pressure-composition (P-C) isotherm measurements of nanocrystalline $Pr_5Co_{19}$ hydrides. The crystal structure and hydrogenation properties of $Pr_5Co_{19}$ are investigated by X-ray diffraction, refined using Rietveld method, and by transmission electron microscopy (TEM). This intermetallic compound crystallizes in the rhombohedral (3R) with $Ce_5Co_{19}$-type structure.

The pressure-composition isotherm of $Pr_5Co_{19}$ was measured at room temperature. A single plateau was observed during the absorption-desorption process, the reversible hydrogen capacity reached 10 H/f.u (0.4 H/M). A peak broadening was observed in the X-ray diffraction (XRD) profile after hydrogenation, with no detection of any amorphous phase.

The crystal structure of the $Pr_5Co_{19}H_x$ hydrides has not been changed, it always conserves the rhombohedral structure (space group $R\bar{3}m$). The lattice parameters have increased with hydrogen content leading to an anisotropic expansion of the unit cell volume.

## I. INTRODUCTION

Rare earth (R) and transition metal (T) based intermetallic compounds have been investigated as hydrogen storage materials[1–4]. Hydrogen absorption in $RT_5$ and $RT_2$ compounds have also been the subject of considerable research[5–10].

For Pr-Ni systems, the $PrNi_2$ phase becomes amorphous after hydrogenation at 323 K and decomposes into $PrH_2$ and $PrNi_5$ after hydrogenation at 773 K[11]. $PrNi_5$ presents two plateaus in the absorption process, the hydrogen capacity reached 1.0 H/M[12,13]. In the Pr-Ni diagram phase, the existence of $Pr_5Ni_{19}$ was recently reported[14,15]. It shows a single plateau between 0.3 and 1.0 H/M and the maximum hydrogen capacity reaches 1.1 H/M. For the desorption process three plateaus are observed. In this case, only 0.3 H/M of hydrogen remains in the sample which presents a reversible hydrogen capacity of 0.8 H/M. The reversible hydrogen capacity is therefore lower than the maximum hydrogen content after the absorption process. Many studies were based on the crystal structures of the Pr-Co binary compounds : $Pr_2Co_{17}$, $PrCo_5$, $Pr_5Co_{19}$, $Pr_2Co_7$, $PrCo_3$, $PrCo_2$, $Pr_2Co_{1.7}$ and $Pr_3Co$. These alloys have been extensively studied[16–20].

$PrCo_3$ and $Pr_2Co_7$ exist as intermetallic compounds with intergrowth structure[5,21,22]. They can be obtained by stacking the $CaCu_5$- and the $MgCu_2$ or $MgZn_2$-type units along the c-axis. $PrCo_3$ presents a rhombohedral structure with $PuNi_3$-type structure (space group $R\bar{3}m$), the lattice parameters are $a = 5.069$ Å and $c = 24.795$ Å[21]. It's important to note that the $PuNi_3$-type structure has three blocks stacked along the c-axis. Each block consisting in the stacking of one $CaCu_5$-type unit and one $MgCu_2$-type unit along the common hexagonal axis[21–23]. Burnasheva *et al.*[24] studied the structure of hydride phases $PrCo_3H_x$. The crystal structure of $PrCo_3H_{1.8}$ was rhombohedral with $a = 5.090$ Å and $c = 27.49$ Å and this structure persisted up to $PrCo_3H_{3.8}$. In the case of $PrCo_3H_{4.8}$ (1.2H/M), the crystal structure became orthorhombic with $a = 9.22$ Å $b = 5.51$ Å and $c = 27.28$ Å.

Concerning the $Pr_2Co_7$ compounds[25], they show two types of crystal structures whose stability depends on the temperature. The first one is a hexagonal $Ce_2Ni_7$-type structure (space group $P6_3/mmc$) with lattice parameters of $a = 5.060$ Å and $c = 24.43$ Å. The second one, is a rhombohedral $Gd_2Co_7$-type structure (space group $R\bar{3}m$) with $a = 5.060$ Å and $c = 36.52$ Å[26]. Goudy *et al.* have studied the hydrogenation properties of $Pr_2Co_7$[27] at 423 K, 448 K, and 473 K. Two plateaus were observed in the absorption process, with plateau

pressures of 0.01 MPa and 0.15 MPa at 423 K. For the same intermetallic system, Iwase *et al.* and Fersi *et al.* studied the hydrogenation properties[28,29]. The hydrogen capacity reached 0.8 H/M at 2 MPa and two plateaus were observed in the absorption-desorption cycle at 413 K.

The intermetallic $PrCo_5$ has been studied by Kuijpers[16]. The maximum hydrogen capacity is equal to 0.6 H/M at 294 K. The enthalpy of hydride formation in this compound is about -38.5kJ/mol $H_2$ deduced from the Van't Hoff plot.

For $Pr_5Co_{19}$, as shown in figure 4, the rhombohedral structure is built from three blocks composed by one $MgCu_2$-type unit and three $CaCu_5$ units. Yamamoto *et al.* reported the crystal system of intermetallic compound $La_5Ni_{19}$ with a $Ce_5Co_{19}$-type structure[30]. The hydrogenation properties of this phase is not clear because the P-C isotherm was measured for a multi-phases sample containing both $La_5Ni_{19}$ and $LaNi_5$. However, there have been only few reports on $R_5Co_{19}$-type compounds.

These materials can be prepared by different techniques. The less time consuming method consists in mechanical alloying with a subsequent annealing[20,31]. High energy milling techniques have been used to produce nanocrystalline powders. The insertion of a light element such as N, C and H is very attractive for many technology applications[32,33]. It results in an increase of the lattice parameters and thus of the unit cell volume.

The present study focused on the crystal structure and hydrogen absorption-desorption properties of $Pr_5Co_{19}$. The intermetallic compound has been synthesized and characterized for the first time by A. E. Ray *et al.*[34], but investigations on hydrogen absorption properties have not been reported yet. P-C isotherms were measured in order to study the hydrogenation properties of nanocrystalline $Pr_5Co_{19}$. The evolution of the crystal structure upon hydrogenation was investigated by means of X-ray diffraction.

## II. EXPERIMENT

A nanocrystalline $Pr_5Co_{19}$ alloy was prepared by arc melting from appropriate amounts of pure Pr and Co (99,9%) under a highly purified Ar atmosphere. Milling was performed for 5 h with ball to powder ratio of 15/1 in a high-energy ball milling[35,36]. The powders, wrapped in tantalum foil, were annealed for 30 min in sealed silica tube under $10^{-6}$ torr at 1073 K[23]. The $Pr_5Co_{19}$ hydrides were prepared by solid-gas reaction using Sievert's method[37,38]. The

hydrogenation properties were measured by determination of the P-C isotherm curves for pressure range between 0.1 and 10 MPa at 298 K, 350 K and 400 K. About 300 mg of intermetallic powder was introduced in the sample holder. It was primary vacuumed and connected to a hydrogenation device with gauged volumes. During absorption, while opening the sample holder, the measured hydrogen pressure decreases[39]. The hydrogen content was obtained with a volumetric method using NIST equation[40].

The final products were characterized using powder X-ray diffraction (XRD) on a Bruker D8 diffractometer. The used wavelength is the average wavelength of Cu $K_{\alpha 1}$ and $K_{\alpha 2}$ with data collected by 0.015° step and analyzed by Rietveld method[41–44]. The reliability of fitting was judged from the 'goodness-of-fit' indicators[43,45–47] $R_B$ and $\chi^2$ :

$$R_B = \frac{\sum_K |I_K(o) - I_K(c)|}{\sum_K I_K(o)}$$

and

$$\chi^2 = \frac{\sum_i w_i |y_i(o) - y_i(c)|^2}{N - P + C}$$

$I_K(o)$ is the observed Bragg intensity and $I_K(c)$ is the calculated one. $N$ is the number of measured points in the diagram, $P$ the number of refined parameters and $C$ the number of constraints.

The sample for TEM observations was not prepared by the classic way that consists to crush a small amount of powder dispersed in a solvant then deposit a drop of the mixture on a carbon film supported by a copper grid. A lamella was prepared by focused ion beam (FIB) using a FEI Helios Dual Beam from the powder sample set in a hard resin. A light mechanical pre-polishing was achieved in order to emerge some grains of the hard resin. Figure 1 shows the main steps of the FIB procedure. The TEM analyses were carried out with a Field Emission Gun FEI Titan Cs-corrected transmission electron microscope (TEM) operating at 200 kV allowing a point-to-point resolution of 1Å. Electron Diffraction and HREM simulations were calculated using the TEM software package JEMS[48].

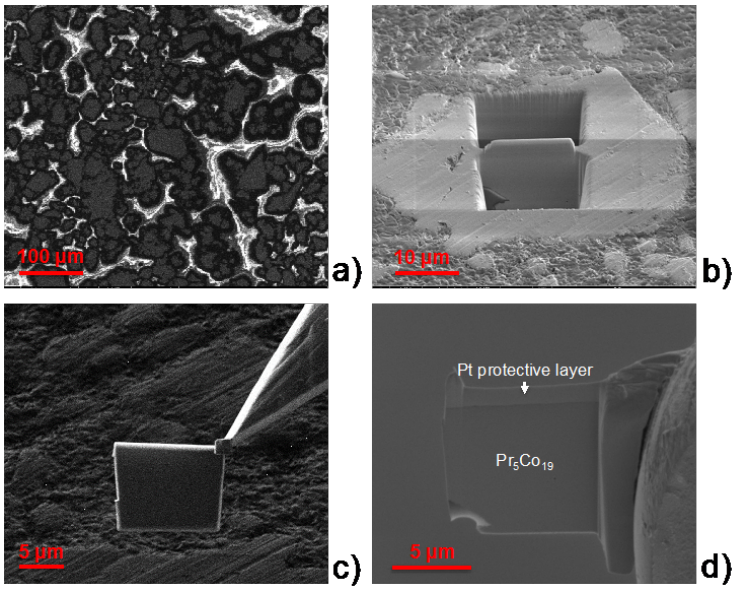


FIG. 1. SEM images showing the main steps of the FIB preparation. Image of the pre-polished powder sample fixed in a hard resin (a). Ion milling of a lamella into a grain (b) then lift out (c) and setting on a copper holder (d).

## III. RESULT AND DISCUSSION

### A. Crystal structure of $Pr_5Co_{19}$

One of the fundamental points of interest in this binary phase system is its crystal feature, the $A_5B_{19}$ crystallizes in the $AB_y$ model described by Khan[49,50], where $y = (5n+4)/(n+2)$, and in this paper A=Pr, B=Co. From the $AB_5$ Haucke and $AB_2$ Laves blocks, the $AB_y$ phase is described as the stacking along the c axis of $[AB_5]$ and $[A_2B_4]$ units following two possible cases : one in $R\bar{3}m$ rhombohedral symmetry (R), obtained by the stacking of $3 \times (n \times [AB_5] + [A_2B_4])$ and the second is the $P6_3/mmc$ hexagonal symmetry (H), formed by the stacking of $2 \times (n \times [AB_5] + [A_2B_4])$ (figure 4).

In the literature, it has been reported that the rhombohedral phase was stable at high temperature, while the hexagonal phase was stable at low temperature[49]. Buschow *et al.* synthesized the compounds $A_2Ni_7$ (A= La, Ce, Pr, Nd, Sm, Gd, Tb, Dy, Ho, Er and Y) by fusion and annealing[5]. They observed, for (A= Pr, Nd, Sm, Gd, Tb and Dy), a modification of ratio between the rhombohedral and hexagonal phases with the annealing temperature. In addition, Buschow *et al.* have also identified that the quantity of R and H phases varied

with the radius of A. A small radius tends to favor the formation of the R phase, whereas for a larger radius the H phase is favored[51].

It's worthy to note that, in general, the $A_5B_{19}$ compounds crystallize in two polymorphic forms : the hexagonal $Sm_5Co_{19}$-type structure and the rhombohedral $Ce_5Co_{19}$-type structure[49]. However, in our case, whatever the annealing temperature, the nanocrystalline $Pr_5Co_{19}$ crystallizes only in the rhombohedral structure (figure 2). The Rietveld refinements performed for samples annealed at 550 °C, 775 °C and 1050 °C confirm the presence of the unique rhombohedral phase with the same lattice parameters. However, for an annealing temperature higher than 1050 °C, $PrCo_5$ phase appears.

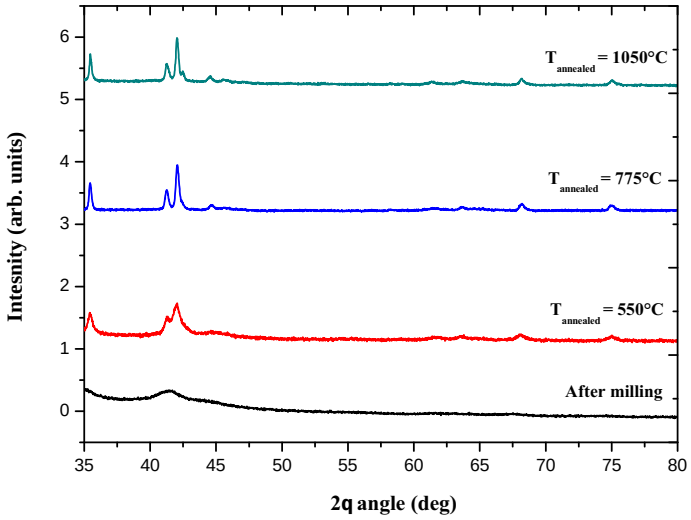


FIG. 2. XRD patterns of $Pr_5Co_{19}$ compound as milled, annealed at 550 °C, 775 °C and 1050 °C.

The fundamental building units of this crystal structure are $PrCo_5$ ($CaCu_5$-type structure) and $PrCo_2$ ($MgCu_2$-type structure) blocks, which are given in figure 4. Let's notice that the unit cell for the rhombohedral structure contains two equivalent crystallographic sites, for Pr, namely $6c$ and $3a$. The Co atoms occupy three crystallographic sites, $6c$, $18h$ and $3b$, the lattice parameters[23] were $a = b = 5.0672\ (4)$ Å and $c = 48.755(4)$ Å .

Figure 3(a) presents the XRD patterns of $Pr_5Co_{19}H_x$ ($x$ = 0, 0.15, 1.5 and 8). We can observe that the diffraction peaks are shifted downward, which means that the unit cell parameters increase and consequently an expansion of the unit cell volume occurred with increasing of the hydrogen content. Figure 3(b) shows the diffractogram for a sample

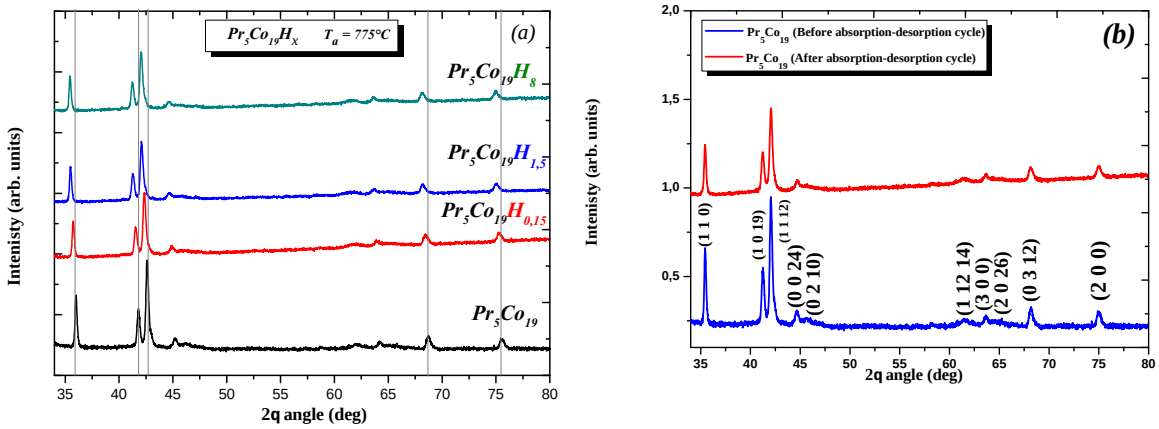


FIG. 3. (a) XRD patterns of nanocrystalline $Pr_5Co_{19}H_x$ ($x = 0$, 0.15, 1.5, 8) compounds, annealed at 775 °C (b) XRD patterns of nanocrystalline $Pr_5Co_{19}$ before (blue) and after (red) absorption-desorption cycle at 293 K

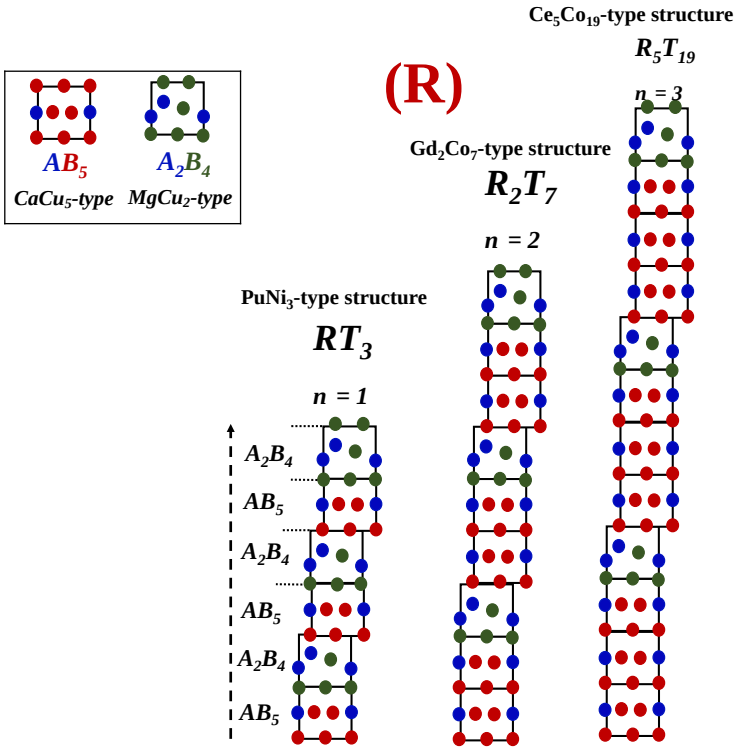


FIG. 4. Crystal structures of $RT_3$, $R_2T_7$ and $R_5T_{19}$ compounds with rhombohedral structure.

obtained after process of absorption-desorption cycles at 293 K, there was no changes in the

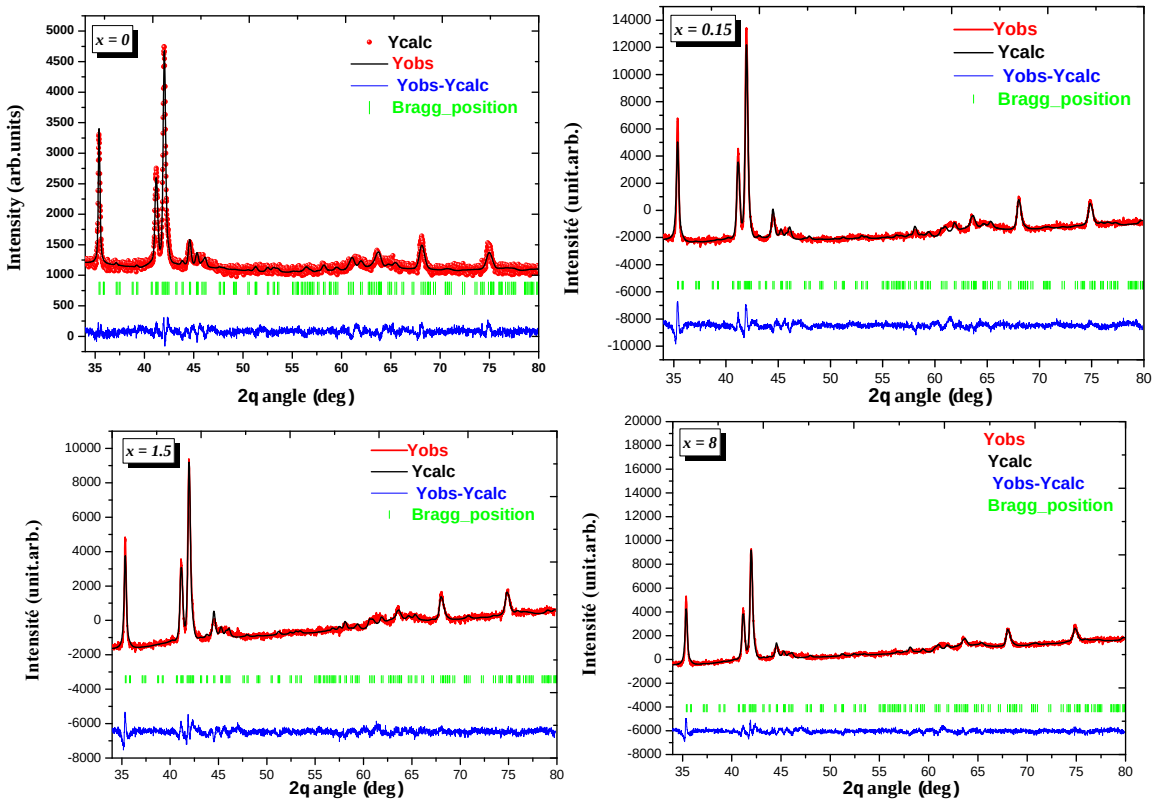


FIG. 5. Rietveld analysis for X-ray diffraction pattern of $Pr_5Co_{19}H_x$ compound ($x = 0$, 0.15, 1.5, 8).

crystallographic structure, reflecting that the $Pr_5Co_{19}$ compound totally desorbed hydrogen, suggesting that this compound is able to absorb hydrogen reversibly.

Rietveld refinements for hydrides $Pr_5Co_{19}H_x$ ($x = 0$, 0.15, 1.5, 8) are shown in Figure 5. One can see that these hydrides conserve the rhombohedral structure for all samples. After hydrogenation, peak broadening was observed in the XRD profile along with some clear Bragg peaks. The structure was not amorphous and the Bragg peaks could be indexed as the $Ce_5Co_{19}$-type structure of the original alloy. The best goodness-of-fit parameters $R_B$ and $\chi^2$ demonstrate that the hydrogen may be located in $9e$ and $36i$ sites. Figure 6 presents the hydrogen atoms crystallographic sites for $Pr_5Co_{19}H_x$. It's important to note that the unit cell parameters will be influenced with insertion of H atoms.

Let's notice that $a$ varies from 5.0672 (4) Å for ($x = 0$) to 5.0863 (3) Å for ($x = 8$) and $c$ is equal to 48.755 (4) Å for $Pr_5Co_{19}$, $c = 48.869$ (3) Å for $Pr_5Co_{19}H_8$. Upon hydrogenation, the unit cell volume expansion $\frac{\Delta V}{V} = \frac{V_H - V}{V}$ is about 0.99% for $x = 8$. $V_H$ and V are the unit cell volume of $Pr_5Co_{19}H_8$ and $Pr_5Co_{19}$, respectively. The values of the structural parameters are

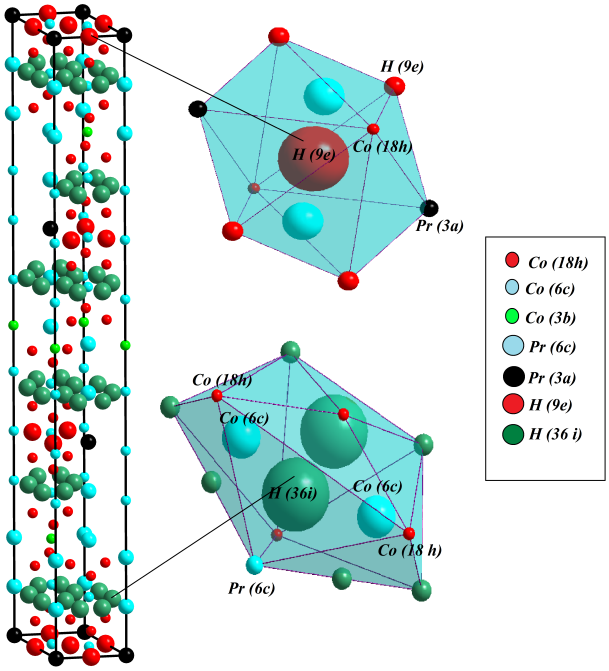


FIG. 6. Crystal structure of $Pr_5Co_{19}H_x$ compound with rhombohedral structure ($R\bar{3}m$ space group) and local environments of H atom.

given in Table I. The same behavior is observed when we compare the $Pr_5Co_{19}H_x$ with the $Pr_5Co_{19}C_x$ carbides[52]. The lattice parameters increased with carbon content : $\frac{\Delta a}{a}$= 0.27%, $\frac{\Delta c}{c}$=1.57% and $\frac{\Delta V}{V}$ = 0.7% for $x = 1.5$.

The grain size was determined from the mean value of the maximum and minimum lengths measured on one hundred different grains (Figure 7-a). The result gave a mean grain size of 120 nm, the minimum and maximum sizes were 32 and 206 nm, respectively. A bimodal distribution was found around the following size values 95 (10%) and 155 nm (7%) (Figure 7-c).

A selected area electron diffraction (SAED) pattern was recorded on a 1 $\mu m^2$ zone on which we have superposed an intensity profile calculated from the XRD refinement (Figure 7-b). The brightest experimental ring was found for $q = 4.6\,nm^{-1}$ also present in the calculated intensity profile corresponding to the (1 1 12) reflection of the ($R\bar{3}m$) rhombohedral $Pr_5Co_{19}$

TABLE I. Unit cell parameters $a$, $c$, and $V$, $R_B$ and $\chi^2$ factors derived from Rietveld refinement for $Pr_5Co_{19}H_x$ ($x = 0, 0.15, 1.5, 8$).

| $x$ | $x$ =0 | $x = 0.15$ | $x = 1.5$ | $x = 8$ |
|---|---|---|---|---|
| $a$ (Å) | 5.0672 (4) | 5.0708 (3) | 5.0723 (3) | 5.0863 (3) |
| $c$ (Å) | 48.755(4) | 48.844(3) | 48.825(3) | 48.869(3) |
| $c/a$ | 9.622 | 9.632 | 9.624 | 9.607 |
| V(Å)$^3$ | 1084.14 | 1087.69 | 1087.718 | 1094.883 |
| $\chi^2$ | 1.98 | 3.33 | 2.57 | 2.44 |
| $R_B$ | 9.68 | 7.18 | 5.85 | 8.59 |
| $z\{18h\}$Co | 0.035 | 0.0414 | 0.0451 | 0.0452 |
| $z\{18h\}$Co | 0.124 | 0.0127 | 0.1265 | 0.1224 |
| $z\{6c\}$Pr | 0.0858 | 0.0769 | 0.0770 | 0.0763 |
| $z\{6c\}$Pr | 0.1509 | 0.1650 | 0.1673 | 0.1655 |
| $z\{6c\}$Co | 0.2505 | 0.2500 | 0.2500 | 0.2500 |
| $z\{6c\}$Co | 0.3333 | 0.3333 | 0.3333 | 0.3333 |
| $z\{6c\}$Co | 0.4153 | 0.4199 | 0.4221 | 0.4226 |
| $x\{36i\}$H | - | 0.34 | 0.34 | 0.34 |
| $y\{36i\}$H | - | 0.0126 | 0.0127 | 0.0126 |

crystal phase.

HREM experiments were investigated in order to characterize the grains individually at the atomic scale. A first experimental image was recorded in [210] projection allowing to distinguish the different atomic stacking planes along c which is the longest axis (Figure 8-a). The HREM simulation done using the XRD refinement shows the same features than the experimental image. Indeed, the brightest dots form the corners of rectangular geometric patterns whose the longest lengths are spaced by lighter dots aligned along c (Figure 8-c). No additional reflection was found in the corresponding Fast Fourier Transform (FFT), meaning the atoms are well ordered in the ($R\bar{3}m$) rhombohedral lattice, the weak intermediate reflections can be assigned to high order Laue zones. The other information is the absence of linear or planar fault, that was also confirmed with another experimental image recorded in [101] projection which contains the atomic stacking planes along the b-axis. This latter

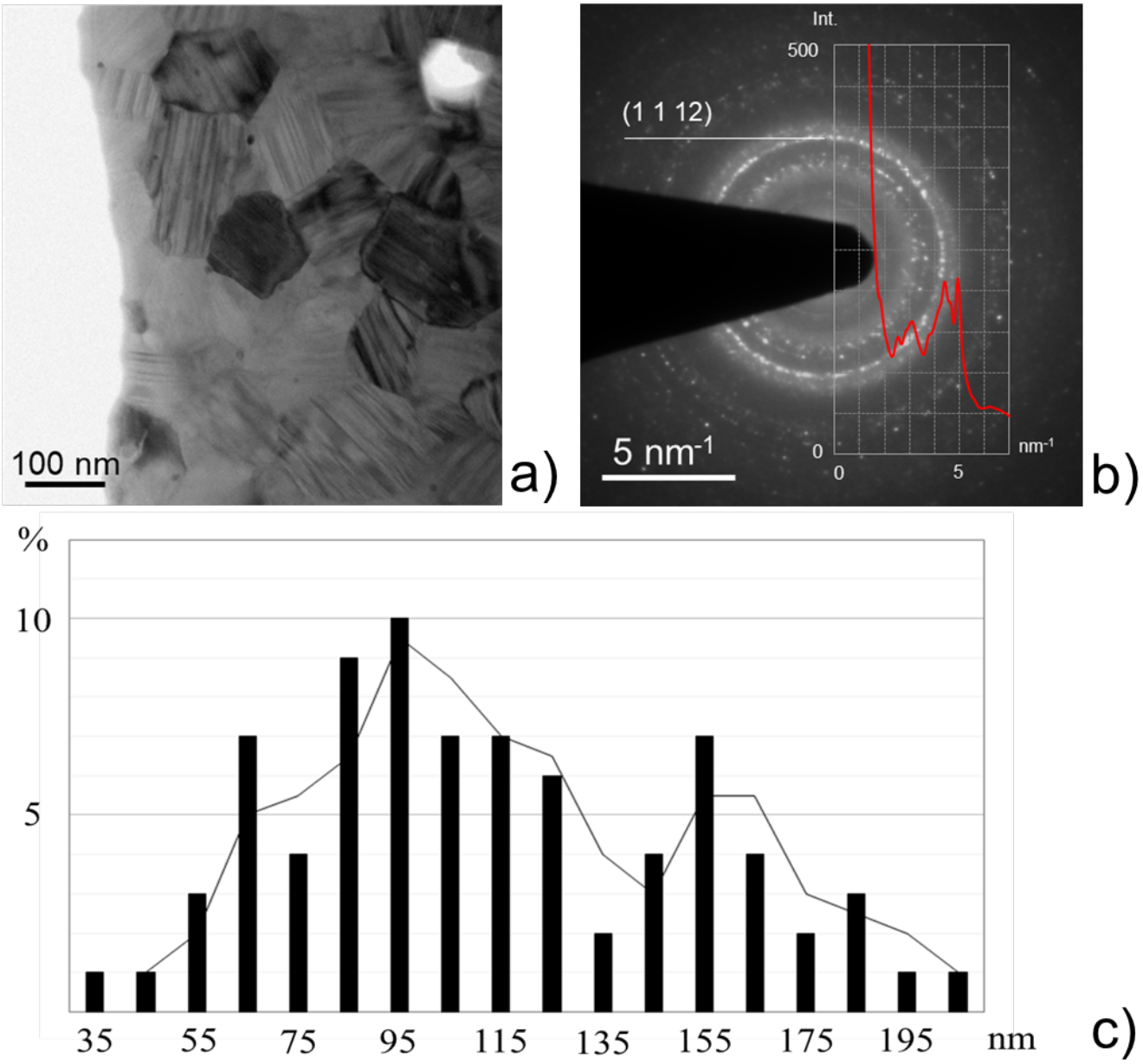


FIG. 7. (a) Bright Field TEM image showing the $Pr_5Co_{19}$ grains, (b) Experimental powder SAED pattern with a simulation of intensity profile (red) done using the structure refined by XRD, (c) Size distribution of the grains.

result can be consulted in additional support (Figure 9).

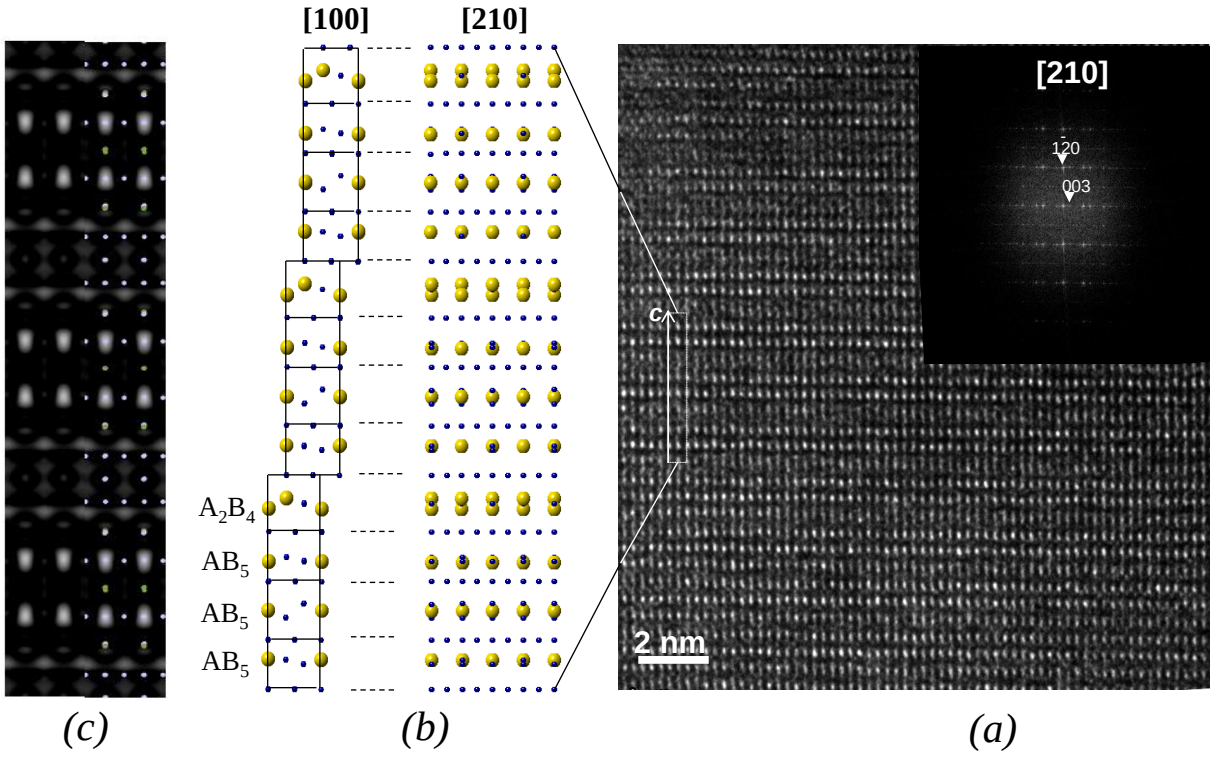


FIG. 8. (a) Experimental HREM image in [210] zone axis with the corresponding FFT. (b) Representation of the $AB_5$ and $A_2B_4$ blocks in [210] projection. (c) HREM simulations with superposition of the Pr (green) and Co (gray) atoms in the right part of the image. The simulation was calculated using the Bloch wave theory for a thickness t = 84 nm, defocus df = -10.6 nm, spherical and chromatic aberration coefficients Cs = -0.03 mm - Cc = 1 mm, respectively. The rectangle in white hashed line corresponds to the simulated area.

### B. P-C isotherms of $Pr_5Co_{19}$

$A_2B_4$ phases are known to absorb large amounts of hydrogen[53] but they undergo hydrogen-induced amorphization[54] especially for B = Ni; on the other hand, $AB_5$ phases have lower capacities, but better cycling stability. Consequently, using alloys composed of $[A_2B_4]$ and $[AB_5]$ subunits is a good way to obtain alloys with both high capacity and good cycling stability. For this reason, we choose to study a $Pr_5Co_{19}$ hydride phase which has

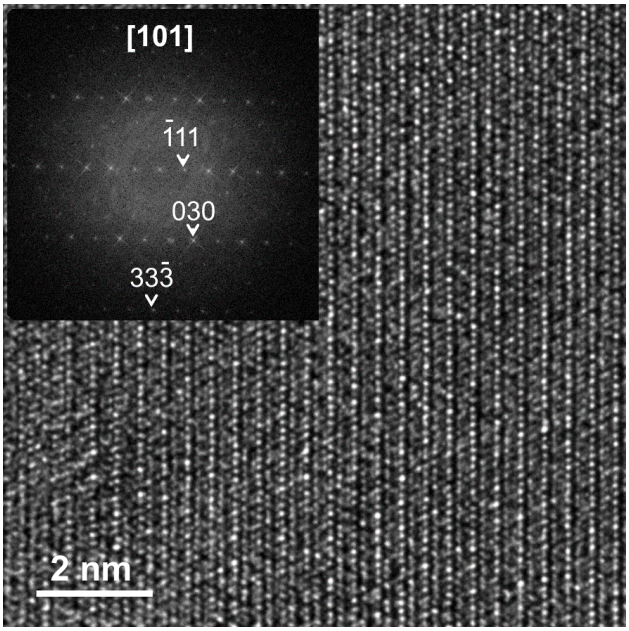


FIG. 9. Additional support : HREM image in [101] projection and corresponding power spectrum.

a low $[A_2B_4]/[AB_5]$ ratio. The volumic expansion of the $PrCo_2$ and $PrCo_5$ units occurring during the absorption-desorption process was refined using the Rietveld method (Figure 10). The hydrogen absorption-desorption properties of nanocrystalline $Pr_5Co_{19}$ is presented in the P-C isotherm measurements (Figure 11). The compound absorbs hydrogen at room temperature. We can observe that only one plateau is identified, in which the solid solution ($\alpha$-phase) and the hydride phase ($\beta$-phase) coexist. The length of the plateau determines the content of stored hydrogen. The pressure of the single plateau is approximately about 1 MPa. The hydrogen capacity reached 0.4 H/M (10 H/f.u).

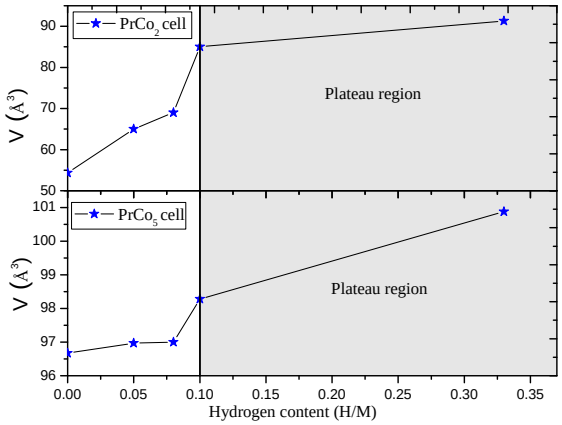


FIG. 10. Expansion of the $PrCo_2$ and $PrCo_5$ units during the absorption process.

Comparing with the $Gd_5Ni_{19}$ ($Sm_5Co_{19}$-type structure), the P-C isotherm at 258 K, shows that the plateau pressures of absorption and desorption were 1.06 and 0.3 MPa, respectively[55]. The hydrogen capacity for $Gd_5Ni_{19}$ is equal to 0.8 H/M.

The synthesis of $Pr_5Ni_{19}$ has been reported by Lemort *et al.*[14]. For this system, the P-C isotherm at 261 K of absorption was different from that of desorption process and the hydrogen capacity reached 1.1 H/M at 7 MPa. This study has been previously reported by Iwase *et al.*[15].

P-C isotherms (PCI) with multiple plateaus have been previously studied for the $RNi_5$ system[12,13,56,57]. Senoh *et al.* measured P-C isotherms for $RNi_5$ (R = La, Pr, Nd, Sm, and Gd) at different temperatures[12]. For Pr, Nd, Sm, and Gd, they observed two plateaus at room temperature. For $LaNi_5$, they observed one single plateau at 298 K and two plateaus at higher temperature. We can conclude that the number of plateaus depends on the temperature and on the nature of the rare earth element.

Van't Hoff plot of the nanocrystalline $Pr_5Co_{19}$ has been obtained from the plateau pressures of the P-C isotherms measured at 298 K, 350 K and 400 K. The PCI prove the formation of a hydride phase by the presence of an equilibrium plateau at all studied temperatures. The plateau pressure for the second cycle at 350 K is about 4.2 MPa. In this case, a plateau region was observed between 0.16 H/M and 0.45 H/M. For the PCI measured at 400 K, a plateau region was identified between 0.18 H/M and 0.37 H/M at 8.7 MPa. The values of the hydrogen capacity for PC-isotherms at 298, 350 and 400 K are reported in Table II. The

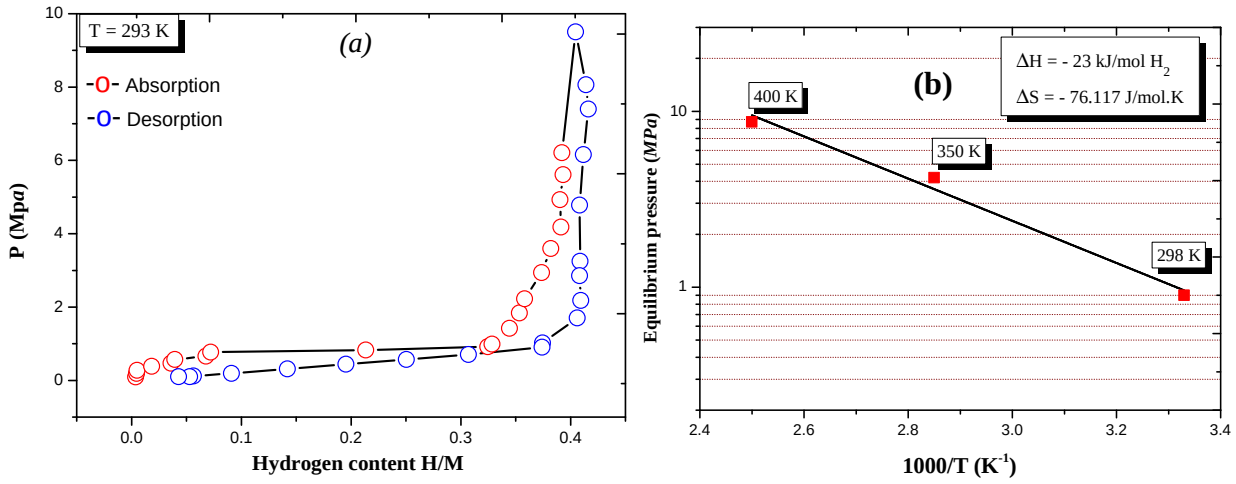


FIG. 11. (a) P-C isotherm of $Pr_5Co_{19}$ at 293 K, (b) Van't Hoff plot for the $Pr_5Co_{19}$-H system. The P-C isotherms were measured at 298 K, 350 K, and 400 K.

TABLE II. Plateau pressures and values of the hydrogen capacity for PC-isotherms measured at 298, 350 and 400 K.

| T (K) | Maximal hydrogen capacity (H/f.u) — (H/M) | Pressure of plateau (MPa) |
|---|---|---|
| 298 | 10 — 0.4 | 1 |
| 350 | 6.8 — 0.28 | 4.2 |
| 400 | 4.56 — 0.19 | 8.7 |

Van't Hoff plot of the $Pr_5Co_{19}$-H system is shown in Figure 11-b. The enthalpy of hydride formation is equal to -23 kJ/mol $H_2$. For $Gd_4MgNi_{19}$, the enthalpy of hydride formation is evaluated to be -16 kJ/mol $H_2$, which is higher than that of $Pr_5Co_{19}$[55]. The entropy value $\triangle S$ was calculated, also, from the Van't Hoff plot, it is close to -76.11 J/mol.K $H_2$.

## IV. CONCLUSION

The crystal structure and hydrogenation properties of nanocrystalline $Pr_5Co_{19}$ compound were investigated along the P-C isotherm. The $Pr_5Co_{19}H_x$ compounds can be successfully synthesized by mechanical milling process followed by solid-gas reaction. The praseodymium based 5:19 hydride, crystallizes in the rhombohedral $Ce_5Co_{19}$-type structure with $R\bar{3}m$ space group. The hydrides conserve always the rhombohedral structure for all hydrogen contents. Rietveld refinement of the X-ray diffraction shows that the hydrogen may be located in $9e$ and $36i$ sites.

The plateau was observed in the P-C isotherm of $Pr_5Co_{19}$ during the hydrogen absorption-desorption process at 298 K. A reversible hydrogen capacity reached approximately 0.4 H/M at 1 MPa. The P-C isotherm of $Pr_5Co_{19}$ showed a single plateau in absorption and desorption. This suggests that hydrogen is absorbed and desorbed in all hydrogen sites simultaneously. Nanocrystalline hydrides based on rare earth and transition metal compounds are attractive alloys due to their interesting structure suitable for hydrogen storage.

## V. ACKNOWLEDGMENTS

This work was supported by the National Center for Scientific Research (CNRS), France, the "Ministère de l'Enseignement Supérieur et de la Recherche Scientifique" (LR99ES17)

and by PHC-MAGHREB Project 15/MAG07.

## REFERENCES

[1]A. A. Volodin, C. B. Wan, R. V. Denys, G. A. Tsirlina, B. P. Tarasov, M. Fichtner, U. Ulmer, Y. D. Yu, C. C. Nwakwuo, and V. A. Yartys, Int. J. Hydrogen Energy **41**, 9954 (2016).

[2]N. Nazer, R. V. Denys, V. A. Yartys, W. K. Hu, M. Latroche, F. Cuevas, B. C. Hauback, P. F. Henry, and L. Arnberg, Journal of Power Sources **343**, 502 (2017).

[3]K. Iwase, N. Terashita, K. Mori, S. Tashiro, and T. Suzuki, Int. J. Hydrogen Energy **43**, 1675 (2018).

[4]K. Iwase, T. Ueno, and K. Mori, Int. J. Hydrogen Energy **44**, 23172 (2019).

[5]K. H. J. Buschow and A. S. V. D. Goot, J. Less-Common Met **22**, 419 (1970).

[6]K. H. J. Buschow and H. H. V. Mal, J. Less-Common. Met. **29**, 203 (1972).

[7]V. Paul-Boncour, A. Percheron-Guegan, M. Diaf, and J. C. Achard, J. Less-Common. Met. **131**, 201 (1987).

[8]K. Young, J. Nei, D. F. Wong, and L. Wang, Int. J. Hydrogen Energy **39**, 21489 (2014).

[9]Z. Lodziana, A. Debski, G. Cios, and A. Budziak, Int. J. Hydrogen Energy **44**, 1760 (2019).

[10]C. B. Wan, R. V. Denys, M. Lelis, D. Milcius, and V. A. Yartys, J. Power Sources **418**, 193 (2019).

[11]K. Aoki, T. Yamamoto, and T. Masumoto, Scr. Met **21**, 27 (1987).

[12]H. Senoh, N. Takeichi, H. T. Takeshita, H. Tanaka, T. Kiyobayashi, and N. Kuriyama, Mater. Sci. Eng. B **108**, 96 (2004).

[13]H. Senoh, N. Takeichi, K. Yasuda, and T. A. Kiyobayashi, J. Alloys Compd. **470**, 360 (2009).

[14]L. Lemort, M. Latroche, B. Knosp, and P. Bernard, J. Alloys Compd. **509**, 823 (2011).

[15]K. Iwase, K. Sakaki, J. Matsuda, Y. Nakamura, T. Ishigaki, and E. Akiba, Inorg. Chem **50**, 4548 (2011).

[16]F. A. Kuijpers, Philips Res Rep Suppl **2**, 42 (1973).

[17]A. Ray, Cobalt **1**, 320 (1974).

[18]H. Senoh, N. Takeichi, and N. Kuriyama, Mater. Trans **45**, 2610 (2004).

[19]R. V. Denys, V. A. Yartys, M. Sato, A. B. Riabov, and R. G. Delaplane, Solid State Chem **180**, 2566 (2007).

[20]R. Fersi, N. Mliki, L. Bessais, R. Guetari, V. Russier, and M. Cabie, J. Alloys Compd. **522**, 14 (2012).

[21]K. Younsi, L. Bessais, J.-C. Crivello, and V. Russier, J. Magn. Magn. Mater. **10-15**, 340 (2013).

[22]K. Iwase, K. Mori, S. Shimizu, S. Tashiro, and T. Suzuki, Int J Hydrogen Energy **41**, 14788 (2016).

[23]W. Bouzidi, N. Mliki, and L. Bessais, J. Magn. Magn. Mater. **441**, 566 (2017).

[24]W. Burnasheva, W. Klimeshin, V. Yartys, and K. Semenenko, Neorg Mater **15**, 801 (1979).

[25]R. Fersi, N. Mliki, and L. Bessais, J. Magn. Magn. Mater. **465**, 220 (2018).

[26]K. H. J. Bushchow, Philips Res Rep **26**, 49 (1971).

[27]A. Goudy, W. Wallace, R. Craig, and T. Takeshita, Adv Chem **167**, 312 (1978).

[28]K. Iwase, K. Mori, S. Tashiro, and T. Suzuki, Int. J. Hydrogen Energy **43**, 11100 (2018).

[29]R. Fersi, M. Cabie, N. Mliki, and L. Bessais, Int. J. Hydrogen Energy **44**, 22011 (2019).

[30]T. Yamamoto, H. Inui, M. Yamaguchi, K. Sato, S. Fujitani, I. Yonezu, and K. Nishio, Acta Mater **45**, 5213 (1997).

[31]G. McCormick, J. Ding, E. H. Feutrill, and R. Street, J. Magn. Magn. Mater. **7**, 157 (1996).

[32]L. Bessais, C. Djega-Mariadassou, D. Tung, V. V. Hong, and N. Phuc, J. Alloys Compd. **455**, 35 (2008).

[33]S. Khazzan, N. Mliki, L. Bessais, and C. Djega-Mariadassou, J. Magn. Magn. Mater. **322**, 224 (2010).

[34]A. E. Ray, A. Biermann, R. Harmer, and J. Davison, Cobalt **4**, 90 (1973).

[35]J. X. Zhang, L. Bessais, C. Djega-Mariadassou, E. Leroy, and A.Percheron-Guegan, Appl. Phys. Lett. **80**, 1960 (2002).

[36]S. Khazzan, N. Mliki, and L. Bessais, J. Appl. Phys. **105**, 103904 (2009).

[37]Z. Yamkane, R. Fersi, F. Rachid, R. Moubah, H. Lassri, N. Mliki, and L. Bessais, J. Magn. Magn. Mater. **449**, 461 (2018).

[38]V. Charbonnier, J. Monnier, J. Zhang, V. Paul-Boncour, S. Joiret, B. Puga, L. Goubault, P. Bernard, and M. Latroche, Journal of Power Sources **326**, 146 (2016).

[39]V. Charbonnier, N. Madern, J. Monnier, J. Zhang, V. Paul-Boncour, and M. Latroche, Journal of Power Sources **397**, 280 (2018).

[40]E. Lemmon, A. Peskin, M. McLinden, and D. Friend, Transp. Prop. Pure Fluids **50** (2000).

[41]H. Rietveld, Acta Crystallogr. **22**, 151 (1967).

[42]H. Rietveld, Acta Crystallogr. **2**, 65 (1969).

[43]J. Rodriguez-Carvajal, Physica B **192**, 55 (1993).

[44]L. Bessais, K. Younsi, S. Khazzan, and N. Mliki, Intermetallics **19**, 997 (2011).

[45]L. Bessais, S. Sab, C. Djega-Mariadassou, and J. Greneche, Phys. Rev. B **66**, 054430 (2002).

[46]L. Bessais, S. Sab, C. Djega-Mariadassou, N. H. Dan, and N. X. Phuc, Phys. Rev. B **70**, 134401 (2004).

[47]L. Bessais, E. Dorolti, and C. Djega-Mariadassou, Appl. Phys. Lett. **87**, 192503 (2005).

[48]P. Stadelmann, Ultramicroscopy **21**, 131 (1987).

[49]Y. Khan, Acta Crystallogr. **B30**, 1533 (1974).

[50]Y. Khan, Phys. Stat. Sol. (a) **23**, 425 (1974).

[51]L. Zhang, Y. Q. Ding, Y. Li, Y. M. Zhao, X. Zhao, B. Z. Liu, and S. M. Han, J. Mater. Chem. A **4**, 9419 (2016).

[52]W. Bouzidi, N. Mliki, and L. Bessais, J. Magn. Magn. Mater. **466**, 411 (2018).

[53]J.-M. Joubert, M. Latroche, and A. Percheron-Guegan, Metallic hydrides II **27**, 694 (2002).

[54]K. Aoki and T. Masumoto, J. Alloys Compd. **231**, 20 (1995).

[55]K. Iwase, K. Mori, A. Hoshikawa, and T. Ishigaki, Inorg Chem **50**, 11631 (2011).

[56]K. Young, B. Huang, and T. Ouchi, J. Alloys Compd. **543**, 90 (2012).

[57]H. Senoh, N. Takeichi, T. H. Takeshita, H. Tanaka, T. Kiyobayashi, and N. Kuriyama, Mater. Trans **44**, 1663 (2003).